FULL PAPER

ADVANCED
HEALTHCARE
MATERIALS

www.advhealthmat.c

Check for
updates

Dual Function of Magnesium in Bone Biomineralization

Jinglun Zhang, Lin Tang, Haoning Qi, Qin Zhao, Yan Liu,* and Yufeng Zhang*

Magnesium (Mg^{2+}), as a main component of bone, is widely applied to promote bone growth and regeneration. However, Mg^{2+} can chemically inhibit the crystallization of amorphous calcium phosphate into hydroxyapatite (HA). The underlying mechanisms by which Mg^{2+} improves bone biomineralization remain elusive. Here, it is demonstrated that Mg^{2+} plays dual roles in bone biomineralization from a developmental perspective. During embryonic development, the Mg^{2+} concentration is enriched in the early stage from embryonic day 13.5 (E13.5) to E15.5, but gradually decreases to a stable state in the late phase, after E15.5. Appropriate concentrations of Mg^{2+} can promote the mineralization of bone marrow mesenchymal stem cells, while excessive Mg^{2+} impairs their osteogenesis. The earlier the Mg^{2+} is added, the stronger the observed inhibition of mineralization. In particular, less Mg^{2+} is present in fully mineralized collagen than in poorly mineralized collagen. Furthermore, a high concentration of Mg^{2+} changes the crystalline morphology of HA and inhibits collagen calcification. Functionally, a high-Mg^{2+} diet inhibits bone biomineralization in mouse offspring. Taken together, the results suggest that appropriate regulation of Mg^{2+} concentration over time is vital for normal biomineralization. This study is significant for the future design of bone substitutes and implants associated with Mg^{2+} content.

1. Introduction

With the rapid development of bioengineering, bone defects and bone loss caused by trauma, congenital skeletal deformities,

infections, and biochemical disorders could be addressed with a wide variety of bone substitutes or implants.[1] Bone is a mineralized composite of inorganic and organic units, mostly hydroxyapatite (HA) and type I collagen, respectively.[2] To mimic the nature of bone, scientists have researched several aspects of the biomaterials of bone substitutes or implants over the past decades,[3] and chemical composition of them is a primary consideration. Currently, magnesium (Mg^{2+}) and Mg^{2+} alloys are gaining increasing research interest due to their promising merits, such as biodegradability, relatively slow corrosion rates, and suitable mechanical properties.[4] However, the osteoinductive effect of Mg^{2+} alloys could not be directly determined due to complex alloy constituents, complicated surface modification technology, and intricate physiological microenvironments.

A bone mineral precursor, amorphous calcium phosphate (ACP), could be fabricated with Mg^{2+} ions, which act as an ACP phase stabilizer to maintain a noncrystal phase.[5] Mg^{2+} could partially substitute Ca^{2+} ions in the apatite structure and inhibit ACP transformation into HA.[5a] Chemically, it has been shown that Mg^{2+} ions retard the crystallization of ACP and control the final aging of crystals.[5c] Moreover, Mg^{2+} is considered the main intracellular antagonist of Ca^{2+}.[6] Hence, there is an unreasonable paradox that Mg^{2+} exerts its role during bone formation as an indispensable element due to its inhibitory effects on biomineralization, which were ignored by previous studies.[6,7] Thus, logically, Mg^{2+} is proposed to have a complicated connection with osteogenesis.

To answer this question derived from the field of regenerative and bioengineering medicine, the best approach is to investigate development, which could subsequently guide regeneration.[2,8] Mineralization development is a kind of complex chemical reaction among calcium (Ca^{2+}), phosphate (PO_4^{3-}), Mg^{2+}, and some amino acids.[2] Among the bones in vertebrates, the cranial bone is unique because it provides spaces, support, and protection for soft brain tissues, and has two different developmental mechanisms, namely, endochondral and intramembranous ossification.[9] Therefore, the development of the skull is a proper model.[10] Numerous studies have demonstrated that several kinds of factors play explicit roles during cranial development,[8,9,11] but which elements and how these elements influence the formation and mineralization of the skull, in particular, HA and type I collagen, are not well defined.

Dr. J. Zhang, Dr. H. Qi, Dr. Q. Zhao, Prof. Y. Zhang
State Key Laboratory Breeding Base of Basic Science of Stomatology
(Hubei-MOST) and Key Laboratory of Oral Biomedicine
Ministry of Education
School and Hospital of Stomatology
Wuhan University
Wuhan 430079, China
E-mail: zyf@whu.edu.cn
Dr. L. Tang
Department of Prosthodontics
Peking University School and Hospital of Stomatology
Beijing 100081, China
Prof. Y. Liu
Laboratory of Biomimetic Nanomaterials
Department of Orthodontics
Peking University School and Hospital of Stomatology
National Engineering Laboratory for Digital and Material Technology
of Stomatology
Beijing Key Laboratory of Digital Stomatology
Beijing 100081, China
E-mail: orthoyan@bjmu.edu.cn

Thereinto, Mg^{2+} is essential for bone health and is mainly intaked by the diet. Approximately 60% of Mg^{2+} in the human body is stored in the bone matrix.[6,12] From an epidemiological perspective, insufficient Mg^{2+} intake can lead to osteoporosis, so Mg^{2+} supplementation would promote patient rehabilitation.[7] Additionally, low Mg^{2+} intake in the diet readily leads to bone dysplasia, with poor mechanical strength and loss of bone mineral density.[7,13] On the other hand, some studies showed that high-Mg^{2+} levels could inhibit cell mineralization in vitro.[14] Clearly, there are doubts still waiting to be solved.

Therefore, the purpose of this study was to elucidate the contradictory phenomena from a developmental perspective. We explored the effects of Mg^{2+} on the embryonic development of the skull and verified the observations in vitro. High Mg^{2+} concentration played an inhibitory role at the early stage of bone biomineralization. The appropriate regulation of Mg^{2+} concentration over time was vital for normal biomineralization. These findings enrich our understanding of biomineralization, and people should be advised to control excess dietary Mg^{2+} intake during pregnancy to avoid nutritional osteodysplasia in offspring.

2. Results and Discussion

2.1. Magnesium Concentration Was Not Linear During Osteogenesis

Increasing Mg^{2+} concentration has been reported by chemists to decrease the crystallinity, lattice parameters, grain size, and thermostability of HA,[5a,15] and paradoxically, the controlled release of Mg^{2+} ions from Mg^{2+} alloys promotes osteogenesis in bone tissue engineering.[4] To provide more reliable information, herein, we investigated the dual function of Mg^{2+} in bone biomineralization from a developmental perspective (**Figure 1**a). Cranial bone could develop through both endochondral and intramembranous ossification,[9] which makes it the best model for research. In addition to Ca^{2+} and PO_4^{3-}, metal elements, such as Mg^{2+}, zinc (Zn^{2+}), and silicon (Si^{2+}), are also stored inside of bone.[7,16] Therefore, we collected cranial bones at several time points and investigated the changes in Ca^{2+}, Mg^{2+} (Figure 1b), Zn^{2+}, and Si^{2+} (Figure S1, Supporting Information) contents during cranial bone formation by inductively coupled plasma optical emission spectrometry (ICP-OES). We found that the Ca^{2+} concentration gradually increased while the Mg^{2+} concentration first increased until embryonic day (E) 15.5 and then decreased as development progressed. However, Zn^{2+} and Si^{2+} rapidly increased after E17.5 and E16.5, respectively, consistent with the general trend of Ca^{2+}. This finding was further confirmed by using cell samples under osteogenic induction in vitro (Figure S2, Supporting Information). The Mg^{2+} concentration of bone marrow mesenchymal stem cells (BMMSCs) declined after day 7, accompanied by increasing Ca^{2+} concentrations.

Previous studies have illustrated that the first mineralization centers of the skull are observed as early as E14.5, prior to extensive mineralization (i.e., E15.5).[17] Mitochondria (M) have been demonstrated to be capable of accumulating both Ca^{2+} and Mg^{2+}.[18] To examine the Mg^{2+} distribution during bone mineralization, we performed scanning transmission electron microscopy (STEM) mapping on embryonic cranial bones at

E13.5, E15.5, and E17.5 to represent mineralization phases (Figure 1c). Semiquantitative analysis of mitochondria showed that the Mg^{2+} concentration first increased and then decreased after E15.5. We found that the Mg^{2+} distribution was not linear with the mineralization process. Therefore, we deduced that different concentrations of Mg^{2+} might play different roles during bone development. This deduction was confirmed by an in vitro mineralization assay of BMMSCs with different concentrations of Mg^{2+} since BMMSCs play a crucial role in new bone formation and remodeling processes. Normally, the concentration of Mg^{2+} in extracellular fluid range from 0.75×10^{-3} to 1.25×10^{-3} M.[6,19] Here, we chose a gradient of Mg^{2+} from 0.25×10^{-3} to 16×10^{-3} M to elucidate its effect on mineralization in vitro. CCK8 assay demonstrated that addition of Mg^{2+} from 0.25×10^{-3} to 4×10^{-3} M did not cause significant cytotoxicity (Figure S3, Supporting Information). Alizarin red staining showed that an additional 0.25×10^{-3} M Mg^{2+} could slightly promote mineralization, and the degree of mineralization began to deteriorate when 0.5×10^{-3} M Mg^{2+} was added to the osteogenic medium (Figure 1d,e). Taken together, these results indicate that the Mg^{2+} concentration is not linear with the osteogenesis process and that higher than normal concentrations of Mg^{2+} can inhibit osteogenesis.

2.2. High Magnesium Inhibited Cell Mineralization at the Early Stage

To better understand the nonlinear relationship between Mg^{2+} concentration and bone developmental process, additional 1×10^{-3} M Mg^{2+}-containing osteogenic-inducing medium (OM) was added into the cell culture medium on days 1, 3, 5, 7, 9, 11, and 13 after the beginning of osteogenic induction (**Figure 2**b). Additional 1×10^{-3} M Mg^{2+} is within of the range of physiological acceptability and lower than the standard of hypermagnesemia with 2×10^{-3} M Mg^{2+} in extracellular fluid.[6] Alizarin red S staining (ARS) showed that mineralization was suppressed with an additional 1×10^{-3} M Mg^{2+} compared with the positive control condition without additional Mg^{2+}. Before day 7, the earlier the additional Mg^{2+} was added, the more obvious the inhibition effect was. However, no significant difference in the absorbance value was found when 1×10^{-3} M Mg^{2+} was added after day 7. A similar result was found when BMMSCs were treated with additional 1×10^{-3} M Mg^{2+} for the same duration at the different stages of mineralization (Figure S4, Supporting Information).

To further confirm this phenomenon, we performed reverse-transcription quantitative polymerase chain reaction (RT-qPCR) to test the mRNA expression levels of osteogenic differentiation markers such as collagen1 (Col1), alkaline phosphatase (ALP), runt-related transcription factor 2 (Runx2), and Osterix. BMMSCs treated with the additional 1×10^{-3} M Mg^{2+} had significantly inhibited transcription of markers of early stage osteogenesis such as Col1 and ALP (Figure 2c,d), but Runx2 and Osterix did not decrease below the control level (Figure 2e,f). This result suggested that additional Mg^{2+} mainly affected collagen production and necessary PO_4^{3-} deposition at the early stage of mineralization but did not weaken osteogenic differentiation. It is well known that collagen is the richest protein in the body and provides mechanical toughness.[2] Changes
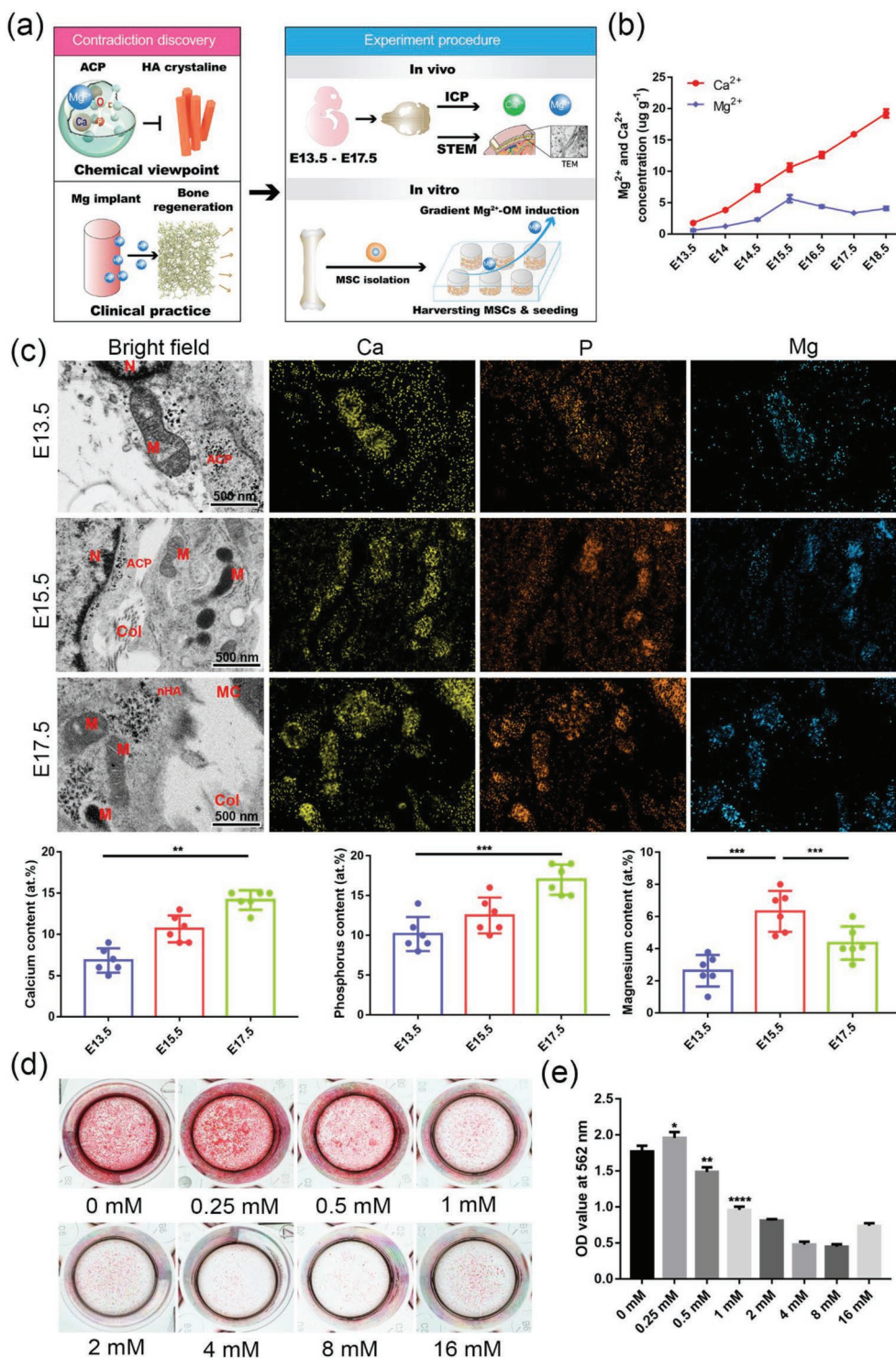
Figure 1. Magnesium concentration was not linear during osteogenesis. a) Schematic illustration of the background paradox and the experimental design. b) Mg^{2+} and Ca^{2+} concentrations of cranial bones harvested at different timepoints. c) Representative images of STEM–EDX elemental mapping of cranial bones collected at E13.5, E15.5, and E17.5 revealed the presence of Ca^{2+}, PO_4^{3-}, and Mg^{2+}. Scale bar = 500 nm. M, mitochondria; N, nucleus; ACP, amorphous calcium phosphate; Col, collagen; MC, mineralized collagen. Higher-resolution images provided in Figure S10 (Supporting Information). The bottom row shows the comparison of elemental compositions (at%) among regions (n = 6 per group) containing mitochondria in the same area in the groups. d) ARS of the mineralization of BMMSCs treated with common OM (containing original 0.8×10^{-3} M Mg^{2+}, shown as 0×10^{-3} M) or containing gradient additional Mg^{2+} concentrations. e) Semiquantification of panel (d) indicated the differences between the control group and the experimental groups. Error bars indicate standard deviation (SD). All of the experiments in panels (b) and (d) were performed at least three times (*$P < 0.05$, **$P < 0.005$, ***$P < 0.0005$, and ****$P < 0.0001$).

ADVANCED
SCIENCE NEWS
www.advancedsciencenews.com
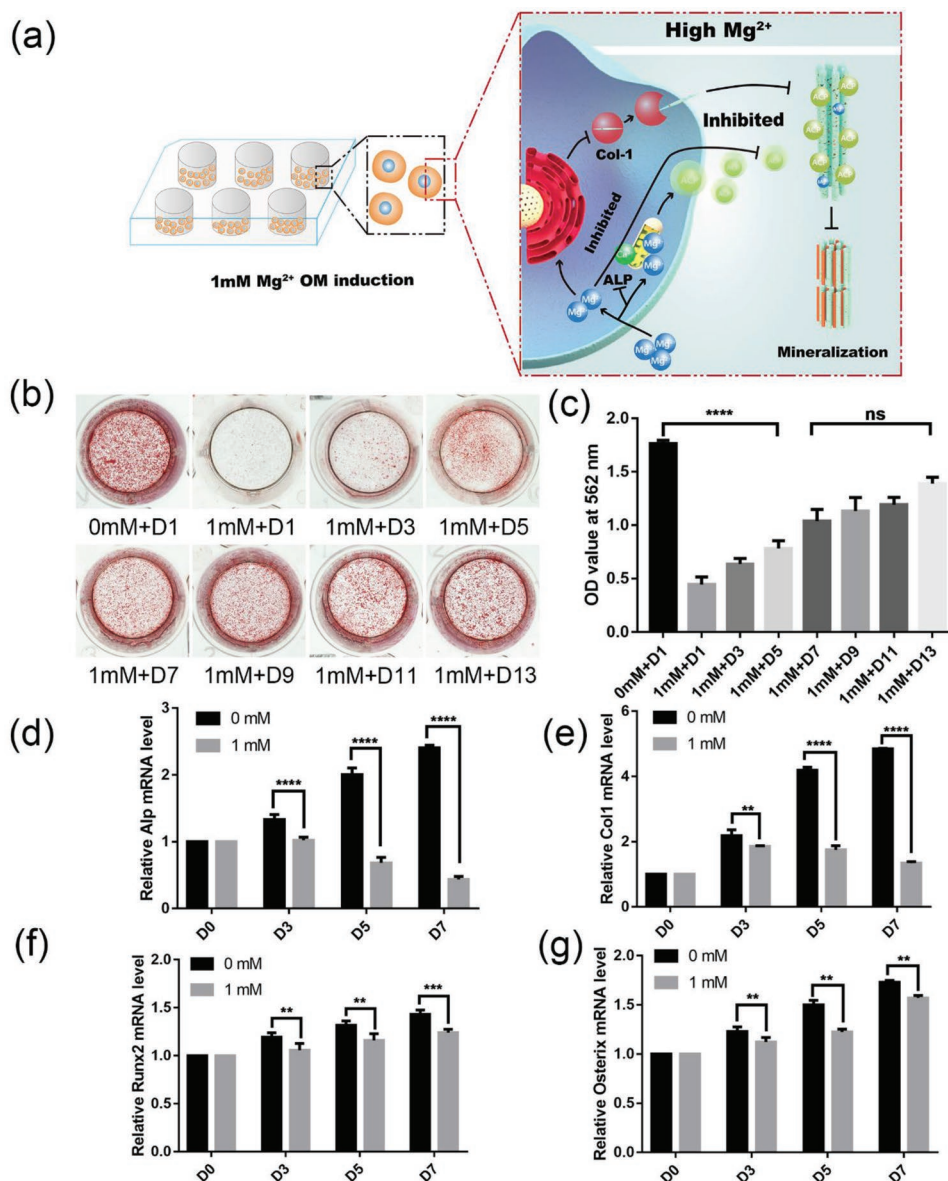
ADVANCED
HEALTHCARE
MATERIALS
www.advhealthmat.de

Figure 2. High-magnesium-inhibited cell mineralization at an early stage. a) Schematic illustration. BMMSCs underwent osteogenic induction by normal OM, and 1×10^{-3} M additional Mg^{2+} OM was administered beginning at a series of timepoints. b) ARS of BMMSC mineralization. Cells were treated with normal OM (containing the original 0.8×10^{-3} M Mg^{2+}, shown as 0×10^{-3} M) at the beginning of the experiment, and the medium was changed to OM containing additional 1×10^{-3} M Mg^{2+} at days 1, 3, 5, 7, 9, 11, and 13. c) Quantification of ARS under an OD of 562 nm. d–g) Relative expression levels of the early osteogenic markers Col1 and ALP and the late-phase osteogenic markers Runx2 and Osterix in BMMSCs cultured in normal OM (shown as 0×10^{-3} M) or extra 1×10^{-3} M Mg^{2+} OM. Error bars indicate SD. All of the experiments were performed at least three times (**$P < 0.005$, ***$P < 0.0005$, and ****$P < 0.0001$; "ns" indicates no significant difference).

in collagen substructure are a significant factor that leads to poor mechanical properties of bone.[20] Moreover, to mineralize bone, osteoblasts secrete intracellular vesicles containing ALP, which decompose the PO_4^{3-} groups that would act as the nucleation center for mineral crystallization.[2] Therefore, low expression of Col1 and ALP stimulated by high Mg^{2+} severely impairs the development of cranial bone due to the lack of raw materials of mineralization. We deduced that overdose of Mg^{2+} could affect activity of ATP-ase and several transcription factors.[6,19,21] Further investigations about the underlying mechanism by which additional 1×10^{-3} M Mg^{2+} suppressed

expression of Col1 would be performed in our future study. Taken together, these results suggest that Mg^{2+} mainly exerts its inhibitory effect in the early stage of mineralization; thus, the Mg^{2+} concentration should not be excessive at this time.

2.3. Appropriate Regulation of Magnesium Concentration Over Time Was of Critical Importance During Bone Biomineralization

Based on the results above, we found that high Mg^{2+} had a significant inhibitory influence on mineralization during the early

ADVANCED
SCIENCE NEWS
www.advancedsciencenews.com

ADVANCED
HEALTHCARE
MATERIALS
www.advhealthmat.de

phase by reducing collagen production and PO_4^{3-} deposition. To explore how Mg^{2+} regulated bone biomineralization, we next microscopically investigated the relationship between normal Mg^{2+} concentration and HA crystallization in vivo by transmission electron microscopy (TEM). Some studies have reported that mesenchymal condensations of the frontal and parietal bones first localize just above the eye and occur at the edges of opposed bones at the sutural margins.[10,11,22] Therefore, we uniformly surveyed this cross section of cranial bones from E13.5 to E17.5.

Calcium phosphate deposits are known to reside as granules in mitochondria.[18b] As shown in **Figure 3**b, numerous intracellular ACP granules and tropocollagen molecules were produced at E13.5. The ACP granules were initially stored in mitochondria and then deposited inside collagen fibrils to form relatively mature mineralized collagen (MC) fibrils at E17.5. Furthermore, the Mg^{2+} levels in mitochondria from E13.5 and E17.5 skull preosteoblasts were similar (Figure 3c), but the mitochondria from E15.5 samples stored most Mg^{2+} ions (Figure 1c). However, the selective area electron diffraction (SAED) data showed that ACP and calcium phosphate granules were amorphous, whereas the Mg^{2+} content of extracellular ACPs was lower than intracellular ACPs (Figure 3d). It was reported that Mg^{2+} served as a typical ACP stabilizer,[23] so we hypothesized that the presence of Mg^{2+} in ACPs could prevent them from transforming into crystals inside the cells in advance.

As far as the collagen region was concerned, the Ca^{2+} concentration increased with mineralization. Moreover, a crystalline diffraction pattern was observed, which corresponded to the 002, 112, 211, and 300 planes of a standard crystalline HA in E17.5, as evidenced by the SAED data in Figure 3b. More importantly, two collagen areas in one visual field had different Mg^{2+} concentrations (Figure 3e). The collagen bundles with a poor degree of crystallization showed higher Mg^{2+} concentrations than the well-mineralized collagens. It seemed that as the collagen matured over time, the Mg^{2+} ions gradually moved away to allow for complete mineralization. Collectively, these data indicate that the proper modulation of intracellular and extracellular Mg^{2+} concentrations over time is so crucial for bone embryonic formation and mineralization.

2.4. Continuous High Concentrations of Magnesium-Inhibited Normal HA Crystallization

Based on these data, it was revealed that under normal development conditions, the concentration of Mg^{2+} gradually decreased in the later stage of mineralization rather than continuing to increase as Si^{2+} and Zn^{2+}. Furthermore, Mg^{2+} ions were well regulated inside and outside of cells until mineralization was complete. Therefore, we next determined why the Mg^{2+} concentration decreased with mineralization maturation by continuous high Mg^{2+} stimulation, disrupting the normal dynamic relationship in vivo. To further investigate whether this kind of treatment affects normal HA crystallization, we performed field emission scanning electron microscopy (FE-SEM) and TEM with mineralized BMMSC samples treated with 1×10^{-3} M Mg^{2+} and collected at different stages of mineralization. Compared to the control cells, the cells treated with

additional 1×10^{-3} M Mg^{2+} produced decreased secretory vesicles at day 3 as shown in the SEM images (Figure S5, Supporting Information). There was less collagen surrounding plate-like granules at day 7 (**Figure 4**b) and day 11 (Figure S6, Supporting Information), indicating that there were insufficient collagen fibrils to provide space for mineral nucleation and propagation. At day 14, the mineralized samples treated with the additional 1×10^{-3} M Mg^{2+} exhibited a change in the morphology of HA crystals from a globoid form to an irregular almond-shaped form (Figure 4b), which was consistent with previous findings.[15a] Specifically, a layered structure gradually evolved after the formation of a varisized staphyline-like structure on day 11. Finally, the lamellar crystals cracked and exposed almond-shaped granules on day 14 (Figure S6, Supporting Information). It was not difficult to determine that Mg^{2+} inhibited HA crystallization and increased the nucleation barrier along collagen fibers, affecting the size and shape of mineral crystals.[8,13,23a]

Additionally, the results acquired by TEM showed that morphologically normal cells were surrounded by a less fibrous extracellular matrix (ECM) in the treatment groups compared with the control groups with native collagen (Figure 4c). This observation was also confirmed by SEM (Figure 4b) and fluorescent images (Figure S7, Supporting Information). Electron-dense deposits enclosed by vesicles contained less Ca^{2+} and more Mg^{2+} in the high-Mg^{2+} groups than in the control groups as determined by point-type energy-dispersive spectroscopy (EDX; Figure S8, Supporting Information). The analysis of mineralized nodules or collagen fibrils at day 14 by SAED indicated that there were textured crystalline diffraction patterns associated with the development of minerals in the control group, while collagen in the high-Mg^{2+} group at day 14 exhibited the amorphous nature of the material. As with the EDX results in vivo, Mg^{2+} was lower in regions with well-mineralized collagen than in other collagen regions where diffraction rings were less well defined (indicating comparatively less crystallinity). These results therefore suggested that continuously excess Mg^{2+} inhibited the effects of mineralization.

The predominant role of collagen in the nucleation, growth, structure, and properties of bone apatites has been intensively studied.[24] Scientists have synthesized intrafibrillarly mineralized collagen (IMC) with a bone-like hierarchical nanostructure in vitro.[25] Further studies are required to confirm whether Mg^{2+} plays a role in IMC formation. Figure 4d showed that a bone-like collagen–mineral hybrid complex formed in the absence of Mg^{2+}. SAED confirmed that the mineral phase was HA. The (002) diffraction was arc shaped and was oriented parallel to the longitudinal axis of collagen in a manner similar to the mineralized collagen property of native bones. However, the collagen mineralized in the presence of 1×10^{-3} M Mg^{2+} showed poor crystallization, which suggested that a continuously high Mg^{2+} concentration would inhibit the mineralization degree of collagen, preventing the completion of mineralization.

Taken together, the results show that Mg^{2+} was maintained at a low level in the early stage to ensure normal collagen production and ALP activity to prepare the raw materials required for mineralization. The concentration peaked as the development progressed. Then, the concentration decreased to ensure normal HA morphology and mature collagen
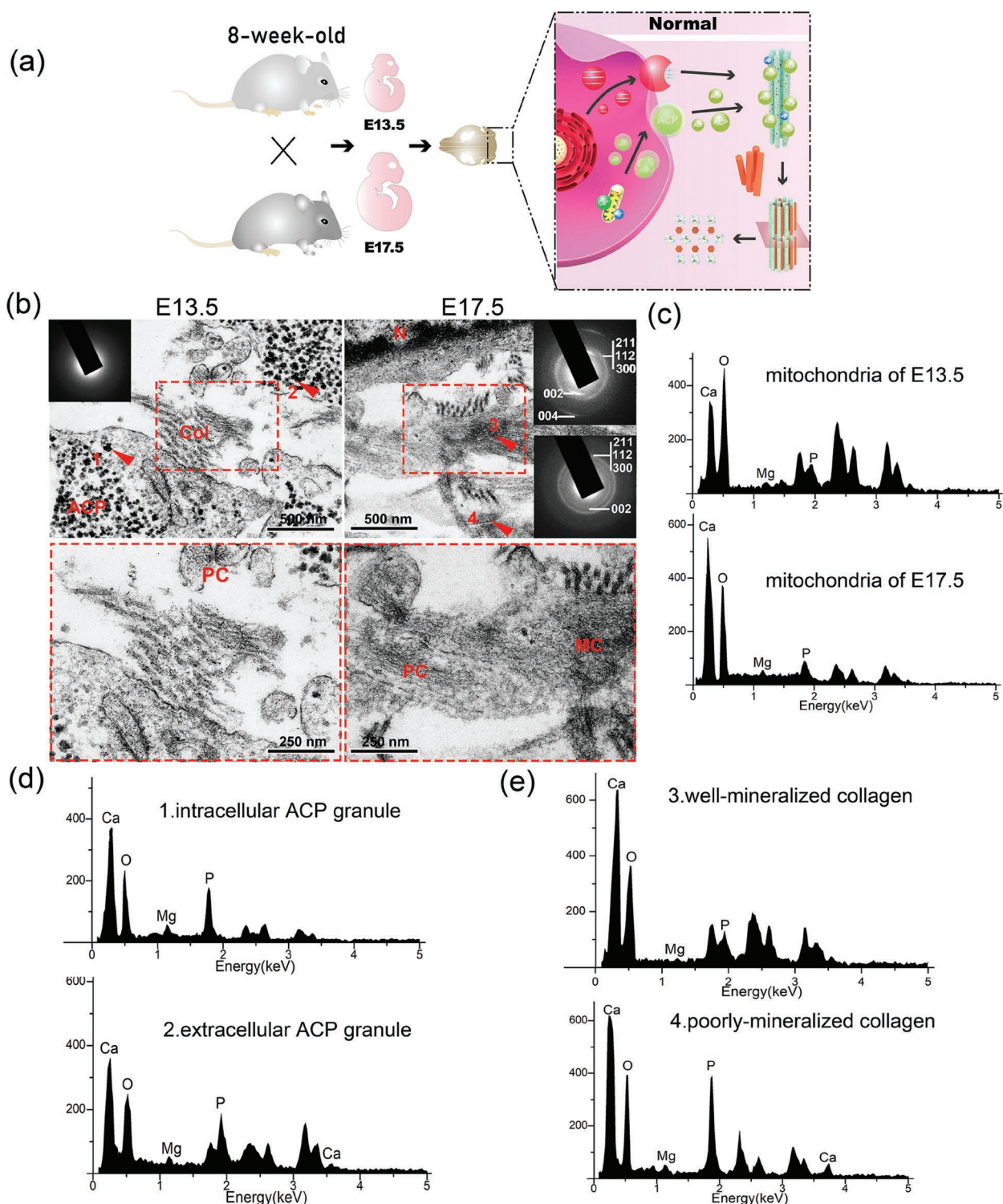
Figure 3. Appropriate regulation of magnesium concentration over time was critically important for bone biomineralization. a) Schematic illustration. b) Representative TEM images of E13.5 and E17.5 cranial bones revealed that intracellular calcium phosphate granules were secreted, procollagen was produced, and collagen was mineralized. The SAED pattern showed that the electron-dense granules were amorphous (inset in left), and the two SAED patterns in the right image correspond to arrowheads 3 and 4. Scale bars = 500 nm (upper row) and 250 nm (lower row). N, nucleus; ACP, amorphous calcium phosphate; Col, collagen; PC, tropocollagen; MC, mineralized collagen. Higher-resolution images provided in Figure S11 (Supporting Information). c) Elemental levels in the mitochondria of E13.5 (upper row) and E17.5 (lower row) cranial preosteoblasts. d) Elemental compositions of ACP at E13.5. The top row and bottom row indicate the ACP sites at arrowheads 1 and 2, respectively. e) Elemental levels of collagens at E17.5. The top row and bottom row indicate the collagen sites at arrowheads 3 and 4, respectively, and the results reveal that greatly mineralized collagen had low Mg^{2+} content. All of the SAED and point-EDX experiments were performed at least six times.
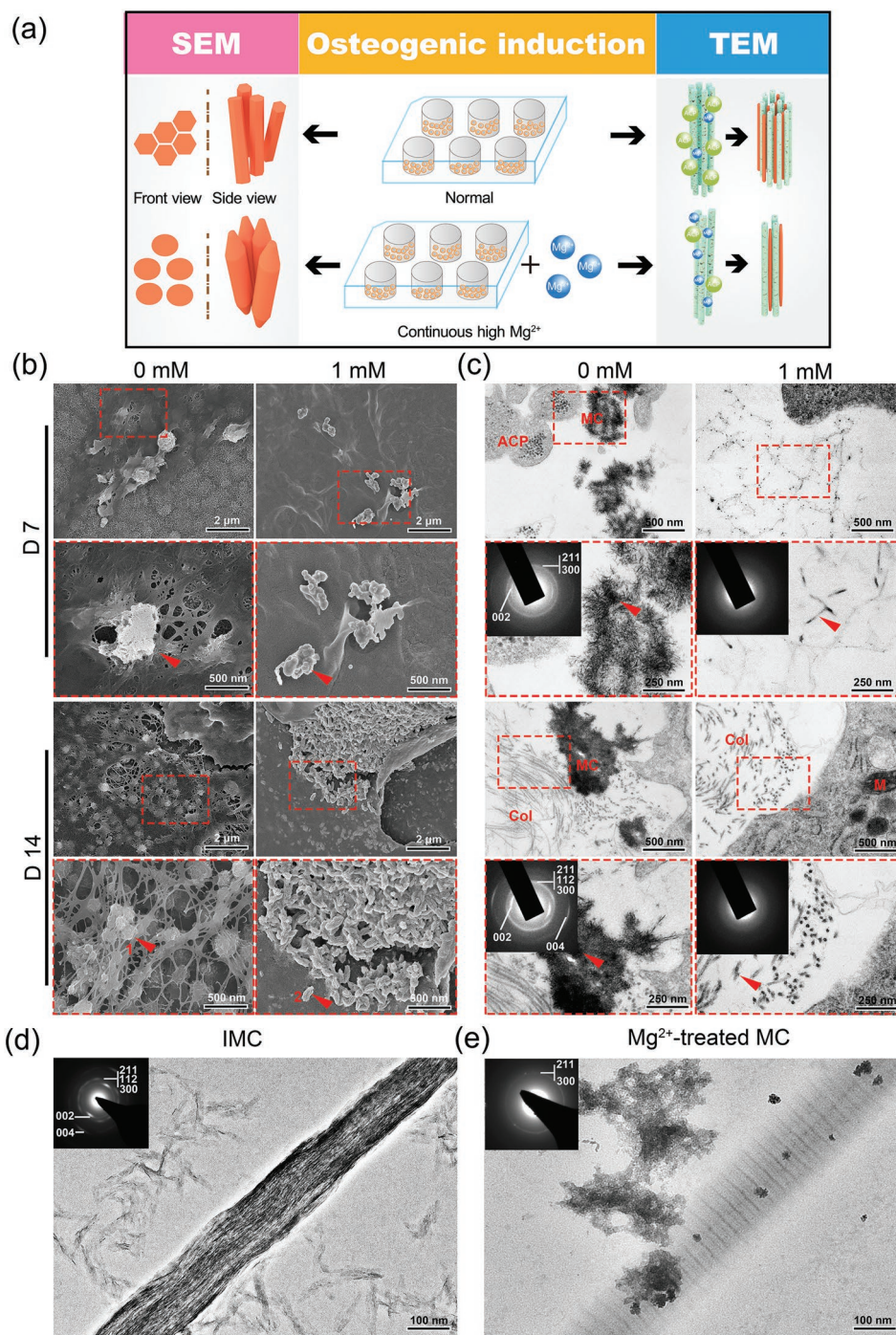
Figure 4. A continuous high concentration of magnesium inhibited normal HA crystallization. a) Schematic illustration. We treated BMMSCs with normal OM and OM containing additional 1×10^{-3} M Mg^{2+} and then harvested the samples on days 3, 7, 11, and 14 for SEM and TEM observation. b) Representative SEM images showing that the BMMSCs mineralized under normal OM and 1×10^{-3} M additional Mg^{2+} OM after 7 and 14 days. Arrowhead 1 shows a normal HA crystal, while arrowhead 2 shows an amygdaloidal one. Scale bars = 2 μm (in rows 1 and 3) and 500 nm (in rows 2 and 4). c) Representative TEM images showing BMMSCs mineralization under normal OM and 1×10^{-3} M additional Mg^{2+} OM at 7 days and 14 days. Scale bars = 500 nm (in rows 1 and 3) and 250 nm (in rows 2 and 4). SAED patterns (inset) represent the crystalline state of the collagen site indicated by the arrowheads. The day 7 and day 14 control groups exhibited ring patterns that were characteristic of apatite, while the SAED in the 1×10^{-3} M additional Mg^{2+} groups showed an amorphous mineral phase even in the day 14 samples. ACP, amorphous calcium phosphate; Col, collagen; MC, mineralized collagen. Higher-resolution images provided in Figure S12 (Supporting Information). d,e) Representative TEM images of collagen mineralized under normal conditions and following treated with 1×10^{-3} M additional Mg^{2+}, respectively. SAED of the fibril (inset) indicated that the crystal was HA. The (002) diffraction plane indicated the orientation of the crystal was parallel to the longitudinal axis of collagen. The (211), (112), and (300) diffraction planes were close to each other, merging into a continuous ring. However, SAED of panel (e) indicated that collagen was much more poorly mineralized. IMC, intrafibrillar mineralized collagen; MC, mineralized collagen.

**ADVANCED
SCIENCE NEWS**
www.advancedsciencenews.com

**ADVANCED
HEALTHCARE
MATERIALS**
www.advhealthmat.de

mineralization; otherwise, a continuous high concentration of Mg^{2+} would occupy the position of calcium ions surrounding collagen and change the size and shape of HA, leading to poor mineralization.

2.5. High-Magnesium Diet Inhibited Mineralization of Bones in Their Offspring

Generally, Mg^{2+} is the second most ample cation in vertebrates and plays a vital role in a number of physiological functions.[23c] Most previous investigations have shown that Mg^{2+} deficiency could impair bone formation and even result in osteoporosis in animal models.[6] Moreover, Mg^{2+} deficiency is mainly attributed to dietary imbalance in offspring. Therefore, to further test how high Mg^{2+} affects offspring bone development, we treated C57/Bl6 female mice with a fixed Mg^{2+}-augmented diet to establish a functionally up-to-requirement model. After 5 weeks of feeding, we measured limb bones, cranial bones, uteruses, and ovaries by ICP-OES (**Figure 5**c,d) to determine changes in Ca^{2+} and Mg^{2+} contents. In comparison to littermates fed a common diet, the mice reared on Mg^{2+}-augmented diet presented decreased Ca^{2+} levels and increased Mg^{2+} levels. Therefore, combined with similar results shown in the in vitro experiment (Figure S9, Supporting Information), Mg^{2+} acted as a Ca^{2+} antagonist in bone, similar to other kinds of tissues[6,18a] and an embryonic development environment with a high-Mg^{2+} level could be established by this method.

Then we collected embryonic cranial bones grown under a high-Mg^{2+} environment. By TEM (Figure 5b), we found delayed development in which fewer intracellular vesicles with low electron density, and preosteoblasts were surrounded by less fibrous ECM and shorter collagen microfibrils. As shown in Figure 5f, collagen regions at E17.5 had poor or no HA crystallization due to excess Mg^{2+} ions. The images also showed that the (002) lattice spacing of the high-Mg^{2+} E17.5 group was 0.326 nm, which was smaller than the (002) lattice spacing of HA (0.34 nm) in the control group. In addition, the Mg^{2+} content of the well-mineralized collagens in the same field of the high-Mg^{2+} E17.5 sample was still lower than that of the poorly mineralized collagens. Consequently, the inhibition of sustained high concentrations of Mg^{2+} was also confirmed in vivo.

To explore the consequences of poor mineralization, we further performed a biomechanical test to determine the strength of bones collected from adult offspring. Figure 5e demonstrates that the stiffness, yield load, work to fracture, and bending modulus of samples from the high-Mg^{2+} diet group were lower than those of samples from the common diet group. Indeed, these data confirmed an undesirable function of bones in response to Mg^{2+} dietary supplementation.

Epidemiologically, nutritionists have linked dietary Mg^{2+} deficiency to osteoporosis. Even moderate Mg^{2+} depletion could result in bone loss.[7] However, some studies clearly demonstrated that Mg^{2+} can block ectopic calcification in skin and vasculature of offspring if the mothers were also fed a diet supplemented with Mg^{2+} during pregnancy.[26] In summary, Mg^{2+} intake should be controlled within a suitable range, and avoidance of excess dietary Mg^{2+} intake during pregnancy should be advised to avoid nutritional osteodysplasia in offspring.

To the best of the authors' knowledge, this is the first study to investigate and elucidate the paradox that increased Mg^{2+} concentrations could decrease the crystallinity of HA, while Mg^{2+} alloys could control the release of Mg^{2+} ions conducive to bone regeneration in vivo. In the fields of development and regeneration, it is generally unreasonable to affirm that Mg-based alloys can promote osteogenesis. Bone substitutes or implants could be designed to stop the release of Mg^{2+} after the initial stage of bone formation. However, the precise control of the release time requires further experimental proof. On the other hand, from a chemical perspective, although Mg^{2+} could competitively occupy the site of calcium and then inhibit the nucleation of ectopic mineralization, Mg^{2+} is still an essential element for organisms. Therefore, further work is still needed to determine the proper concentration of Mg^{2+} for use in clinical applications.

3. Conclusion

The contradictory phenomena of the role of Mg^{2+} in bone biomineralization were explained from a developmental perspective in the present study. We found that the appropriate regulation of Mg^{2+} concentration over time was vital for normal biological crystallization (**Scheme 1**). High Mg^{2+} concentrations impaired the bone mineralization degree by inhibiting the production of collagen and other raw materials required for bone formation, such as calcium phosphate. Moreover, the continuous overdose of Mg^{2+} changed the morphology of HA and retarded the mature crystallization of collagen during the later phases of biomineralization. These findings enrich our understanding of biomineralization and suggest that the control excess dietary Mg^{2+} intake during pregnancy should be advised to avoid nutritional osteodysplasia in offspring. Moreover, these results suggest the great significance of considering Mg^{2+} content in the future design of bone substitutes and implants.

4. Experimental Section

Mice and Treatment: All procedures used in this research were performed in accordance with the policies of the Ethics Committee for Animal Research, Wuhan University, China (ethical approval number 134/2012).

Female and male C57BL/6 mice, 8 and 10 weeks of age, respectively, were purchased from Vital River (Beijing, China). In pregnant mice, the plug date was defined as E 0.5. Before collecting embryos, the pregnant female mice were sacrificed by anesthesia overdose. The embryos were fixed with a mixture of 2% paraformaldehyde and 2.5% glutaraldehyde in 0.1 M phosphate buffer (pH = 7.4) for ultrastructural studies.[17a] The calvaria were sectioned just above the eye at the edges of the opposed bones at the sutural margins, which were ultrastructurally studied by TEM observation.

For harvesting high-Mg^{2+}-conditioned embryos, the female mice were divided into two groups: common diet group and a high-Mg^{2+} group. Both groups were consisted of ten mice and were mated with male mice fed a common diet at 10 weeks of age. The mice were fed a high-Mg^{2+} diet from 3 weeks of age, when they could feed themselves, until 8 weeks of age, when they were able to become pregnant. The mice fed the common diet were maintained on a standard rodent laboratory diet (Laboratory Autoclavable Rodent Diet 5010; PMI Nutritional International, Brentwood, MO, USA) under standard conditions.[26b] The
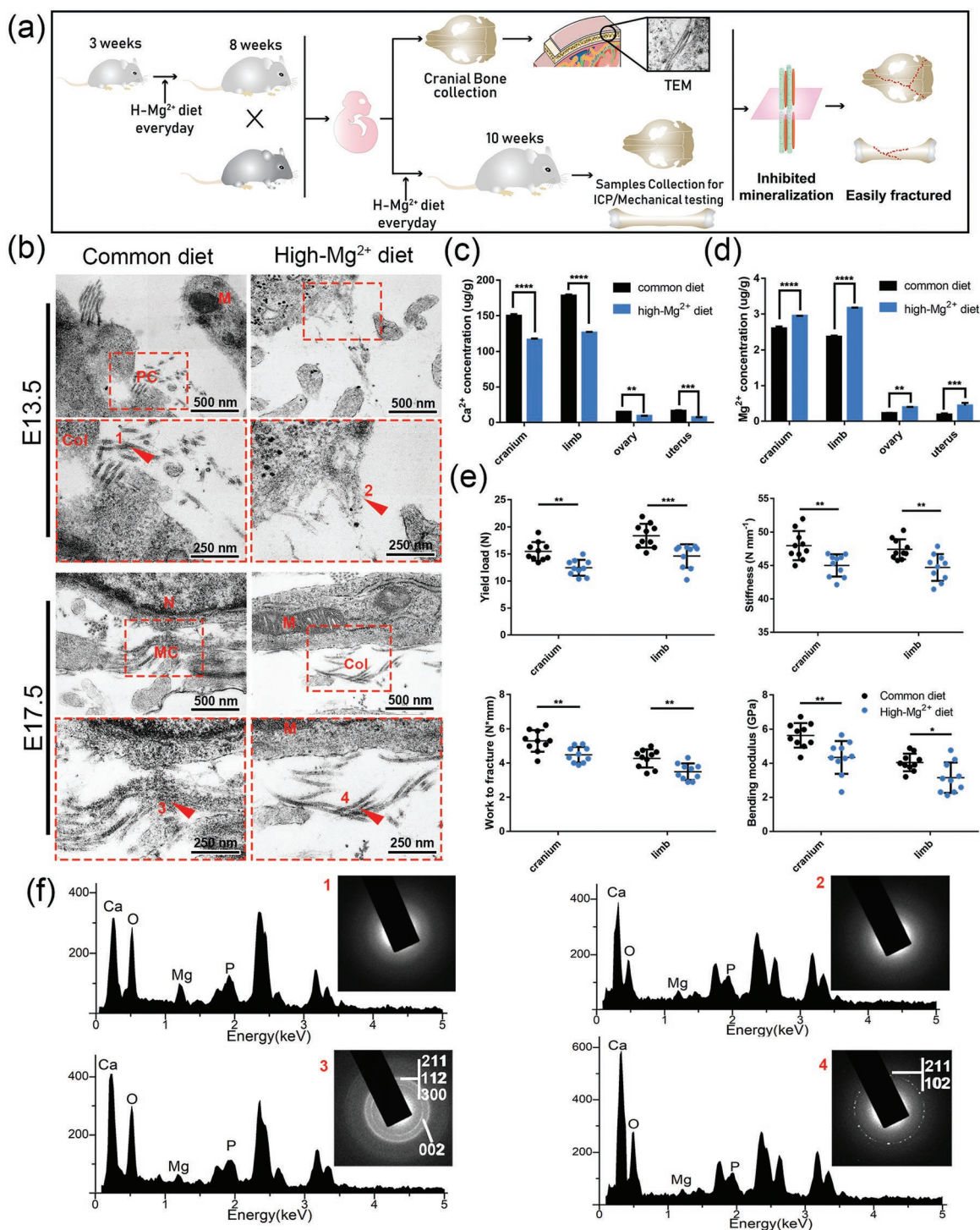
ADVANCED
SCIENCE NEWS
www.advancedsciencenews.com

ADVANCED
HEALTHCARE
MATERIALS
www.advhealthmat.de

Figure 5. A high-magnesium diet inhibited the mineralization of bones in their offspring. a) Schematic illustration. We fed mice a high-Mg^{2+} diet every day and harvested embryos developed under a high-Mg^{2+} environment for TEM of cranial bone. We compared the adult mice grown normally with mice raised by a high-Mg^{2+} diet with respect to mechanical testing. b) Representative TEM images of E13.5 and E17.5 cranial bones collected from the common diet group and the high-Mg^{2+} diet group. Scale bars = 500 nm (in rows 1 and 3) and 250 nm (in rows 2 and 4). M, mitochondria; N, nucleus; Col, collagen; PC, tropocollagen; MC, mineralized collagen. Higher-resolution images provided in Figure S13 (Supporting Information). c) Changes in the Ca^{2+} concentration of cranium, limb, ovary, and uterus after feeding a high-Mg^{2+} diet. d) Changes in the Mg^{2+} concentration of cranium, limb, ovary, and uterus after feeding a high-Mg^{2+} die. e) Mechanical testing of cranial bones and femurs from the common diet group and the high-Mg^{2+} group. Flexural tests of intact bones showed bending modulus and yield load ($n = 10$ per group). f) Point-EDX and SAED of four arrowhead sites. The Mg^{2+} content of well-mineralized collagen was lower than that of poorly mineralized collagen. All of the SAED and point-EDX experiments were performed at least six times, and experiments in panels (c)−(e) were performed at least three times. Error bars indicate SD (**$P < 0.005$, ***$P < 0.0005$, and ****$P < 0.0001$).
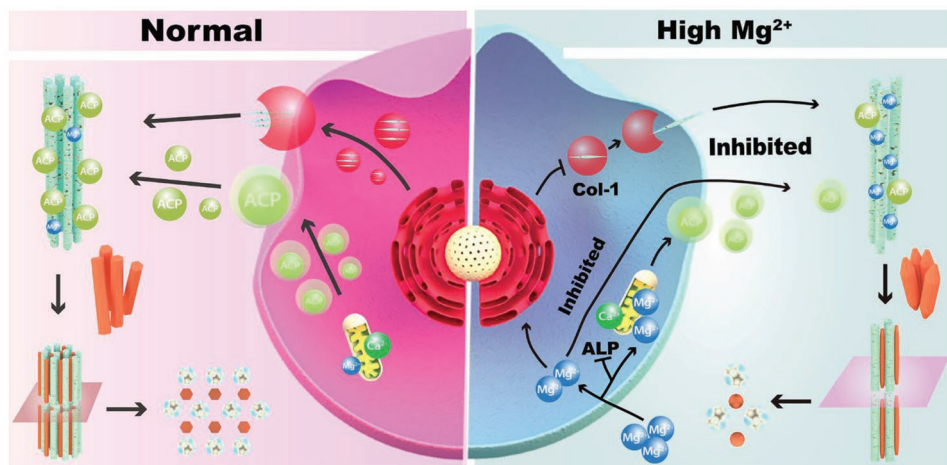
Scheme 1. Schematic of the involvement of magnesium during biomineralization. Calcium ions are stored in mitochondria and reside as ACP granules, and Mg^{2+} also accumulates in mitochondria. Under normal conditions, the mitochondria release ACP accompanied by some Mg^{2+} into intracellular and extracellular matrices when ACP accumulation reaches a threshold. Additionally, the Golgi apparatus secretes Golgi cisterna containing procollagen and transports it to the extracellular space. ACP vesicles are deposited on collagen fibrils and intrafibrillarly convert to additional crystalline apatite in the shape of six prisms, propagating from dense foci. After exposure to high Mg^{2+}, stem cells with osteogenic potential accumulate additional Mg^{2+} in mitochondria and decrease the expression level of Col1 and Alp, leading to the reduced production of collagen and ACP in the early stage of mineralization. A continuous high-Mg^{2+} microenvironment then changes the morphology of HA. In the middle of the scheme is the cell nucleus surrounded by the Golgi apparatus. The Golgi cisterna is red and contain procollagen in cyan. Mitochondria are shown in yellow, Ca^{2+} ions are green, Mg^{2+} ions are blue, and ACP vesicles are light green. HA crystals are orange. The pathways are represented by solid black arrows, indicating release and formation processes, and solid lines with right vertical bars indicating inhibitory effects.

fodders in the high-Mg^{2+} group were supplemented with magnesium chloride at a dose of 100 mg kg^{-1} irrespective of its content in the basal diet. The concentration of Mg^{2+} formulated in fodders was based on that used in a previous study which showed increased Mg^{2+} associated cognitive functional changes without any adverse effects.[27]

To determine the effects of high-Mg^{2+} diet on female mice, calvaria, limb bones, uterus, and ovaries were collected for subsequent experiments. The pregnant mice in the high-Mg^{2+} group were fed with the corresponding diet during pregnancy and the suckling period. The pregnant mice were sacrificed and embryo samples were collected by the same method as described.

To analyze the effects of a high-Mg^{2+} diet on long-term bone development, the offspring from the high-Mg^{2+} group were placed on a high-Mg^{2+} diet for another 6 weeks beginning at 4 weeks of age. Additionally, the next-generation littermates of the common diet group at 10 weeks old were fostered. The mice were sacrificed for subsequent analysis.

Cell Culture and Alizarin Red S Staining: BMMSCs were harvested from the femurs of 6 week old B6/C57 mice using the method described previously[28] after euthanasia by sodium pentobarbital. Briefly, after the femurs were carefully washed, the bone marrow was flushed using alpha Dulbecco's modified Eagle's medium (α-MEM, HyClone). Following 72 h of incubation under a standard culture environment in α-MEM containing 20% fetal bovine serum (FBS; Gibco, Life Technologies Corporation), the adherent cell population was left and grown in culture flasks. The cells were further detached and purified, and the cells in passage 3 were used in the following experiments.

Cells were seeded in 24-well plates for ARS. The OM was composed of α-MEM (containing original 0.8×10^{-3} M Mg^{2+}), 10% FBS, 10×10^{-9} M dexamethasone, 10×10^{-3} M β-glycerophosphate, and 5×10^{-3} M L-ascorbic acid with the following different concentrations of additional Mg^{2+}: 0.25×10^{-3}, 0.5×10^{-3}, 1×10^{-3}, 2×10^{-3}, 4×10^{-3}, 8×10^{-3}, and 16×10^{-3} M. Magnesium chloride hexahydrate (Sigma) was used for cell culture.

In other plates, the same OM supplemented with 1×10^{-3} M additional Mg^{2+} were used from 1st, 3rd, 5th, 7th, 9th, 11th, and 13th days after beginning normal osteogenic induction. So, 1×10^{-3} M Mg^{2+} OM stimulated the BMMSCs lasting 13, 11, 9, 7, 5, 3, 2, and 1 days,

respectively. The culture medium of each group was replaced with fresh inducing medium every other day.

To exclude the effect of duration, the cells were treated for the same 12 h by 1×10^{-3} M Mg^{2+} OM at the different stages (1st, 3rd, 5th, 7th, 9th, 11th, and 13th) and then replaced by common OM to complete mineralization. The culture medium of each group was replaced with fresh inducing medium every other day.

After being induced for 14 days, well plates were washed and then fixed for 10 min and stained by 0.2% Alizarin red S (Sigma-Aldrich) staining solution (pH = 4.2) for 30 min at 37 °C. After taking pictures, Alizarin red was dissolved in 200 µL of 1% cetylpyridinium chloride (Sigma-Aldrich) at room temperature for 2 h and transferred into a 96-well plate to examine the absorbance value at an OD of 562 nm.

Confocal Laser Scanning Microscopy: BMMSCs were seeded on coverslips and mineralized under OM and additional 1×10^{-3} M Mg^{2+} OM for 7 days. To stain fluorescently, stain cells were fixed in 4% paraformaldehyde, permeabilized with 0.25% Triton-X, and blocked by 1% bovine serum albumin (BSA). Subsequently, the primary antibodies against Col1 (A1352, ABclonal Biotechnology Co., Ltd) with 1:100 dilution were dropped onto coverslips and incubated overnight at 4 °C. Then the coverslips were incubated by secondary antibody with a green fluorescent marker for 30 min, followed by 5 min of nuclear staining with 4′,6-diamidino-2-phenylindole (DAPI). The samples were observed with a laser-scanning microscope (InSIGHT Plus-IQ, Meridian, USA).

Quantification of Elements: The elements in the cell and tissue samples were quantified by ICP-OES. BMMSCs were seeded in 10 cm dishes and induced by normal OM (original 0.8×10^{-3} M Mg^{2+}) or OM containing additional 1×10^{-3} M Mg^{2+} (total Mg^{2+} concentration of 1.8×10^{-3} M). The cells were detached by trypsin (HyClone) on days 0, 3, 7, 11, and 14, and washed three times with deionized water. Prior to quantification, the culture suspension or tissues were diluted 7.5-fold with 2% concentrated nitric acid (Sigma-Aldrich).

Cytotoxicity of Mg^{2+} Using CCK8 Assay: The proliferation of BMMSCs was examined using a CCK8 kit (DOJINDO, Japan) after 1, 3, and 5 days of being cultured with the different concentrations of additional Mg^{2+} in OM. Briefly, BMMSCs were seeded at a density of 5×10^3 cells per well in a 96-well plate. At each time point, the medium was removed, replaced with 110 µL solution (containing 10 µL of CCK8 original solution) and

**ADVANCED
SCIENCE NEWS**

www.advancedsciencenews.com

**ADVANCED
HEALTHCARE
MATERIALS**

www.advhealthmat.de

incubated for 1 h at 37 °C. The OD value was immediately quantified by measuring the absorption at 450 nm using a microplate reader.

Ultrastructural Examination: TEM was performed to identify mineral deposits and collagen mineralization. Cells and calvaria samples were collected, fixed with glutaraldehyde, postfixed with 1% osmium tetroxide, dehydrated in an ascending ethanol series, transferred to acetone, and embedded in epoxy resin as previously reported.[18b] After sectioning and staining, the samples were observed by JEM-1400 TEM (JEOL, Tokyo, Japan) at 120 kV. SAED was performed on electron-dense granules and extracellular collagen regions and EDX was used to analyze the element constituents of samples by a TF20-2100F high-resolution TEM (JEOL, Tokyo Japan) at six different points for each sample. The EDX data were calibrated by a matched ZAF quantitative analysis program. To measure the spatial distribution of Ca, Mg, and P within bones, high-resolution quantitative STEM–EDX imaging was performed. The specimens used for STEM mapping were not postfixed. Thin sections were examined with an HT-7700 STEM (Hitachi, Tokyo, Japan) at 100 kV. To quantify the elemental compositions, regions ($n = 6$) of same area that contained whole region of mitochondria by AZtec nanoanalysis system (Oxford Instruments) were selected. Boundary of mitochondria was defined by their membrane structure. The average of the percentages of element content was used for statistical analysis.

Scanning Electron Microscopy: BMMSCs were seeded on sterile glass coverslips (Nest) and induced by normal OM or OM containing additional 1×10^{-3} M Mg^{2+}. Samples were collected on 3, 7, 11, and 14 days, and fixed for 2 h at 4 °C, dehydrated by ascending ethanol series and a critical evaporator. Then coverslips were observed by FE-SEM (SU7000, Hitachi, Japan) under 20 kV. SEM images were obtained at magnification from 5 to 50k at five different field views for each sample.

Synthesis of Mineralized Collagen: The IMC was synthesized as previously reported.[25] Briefly, a single-layer type I collagen was assembled on the formvar-and-carbon-coated Ni TEM grids, which were floated upside down on a 100 µL drop of a mineralization solution and sealed inside a 100% humidity chamber. The mineralization solution was composed of 4.2×10^{-3} M K_2HPO_4, 9×10^{-3} M $CaCl_2 \cdot 2H_2O$, and 0.5 g mL^{-1} polyacrylic acid. To achieve the MC in a high-Mg^{2+} environment, 1×10^{-3} M $MgCl_2$ was added to the mineralization solution. All mineralization was performed at 37 °C for 72 h. Then, each grid was examined with an FEI TECNAL G2 F30 S-TWIN TEM (FEI, USA) at 120 kV after dehydration. The SAED coupled to TEM was used to demonstrate the degree of crystallinity.

Bone Mechanical Testing: Mechanical properties and bone matrix material properties were evaluated by using yield load tests, fracture toughness tests, bending modulus, and stiffness examination as reported in previous studies.[29] Briefly, intact skulls and femurs were isolated from 10 week old second-generation mice from the common diet and high-Mg^{2+} diet groups ($n = 10$ per group). For examination of work to fractures and stiffness, skulls and femurs were positioned on two supports. Displacement was applied transverse to the long axis of the bone at a rate of 0.01 mm s^{-1} until failure.[30] Force displacement data were recorded at 60 Hz. The bending modulus of the samples was examined by compressing to 10% strain with a deformation rate of 1 mm min^{-1}. Then the bending modulus was calculated as the slope of the linear stress–strain curve.

RNA Extraction and RT-qPCR: Total RNA was extracted with TRIzol and series of standard protocols. After the synthesis of complementary DNA, RT-qPCR was performed using Prime-Script RT-PCR Kit (TaKaRa, Japan). The primer sequences of target genes are listed in Table S1 (Supporting Information).

Statistical Analysis: Data were examined for normality and homoscedasticity assumptions. The statistical analyses were performed by GraphPad Prism software 7.0 (GraphPad, USA). One-way, analysis of variance (ANOVA), two-way ANOVA, and Student's *t*-test were used to analyze differences among groups in cell and animal experiments. *P*-values less than 0.05 were considered statistically significant. For each TEM grid in each experimental group, the EDX and SAED data were collected from six different points with similar structures at one field of view to compare the differences between the two groups. The median score was used to summarize the six scores collected from each sample and was shown in the figures.

Supporting Information

Supporting Information is available from the Wiley Online Library or from the author.

Acknowledgements

Conflict of Interest

The authors declare no conflict of interest.

Keywords

[1] Y. C. Chai, A. Carlier, J. Bolander, S. J. Roberts, L. Geris, J. Schrooten, H. Van Oosterwyck, F. P. Luyten, *Acta Biomater.* **2012**, *8*, 3876.

[2] Y. Liu, D. Luo, T. Wang, *Small* **2016**, *12*, 4611.

[3] A. M. Barradas, H. Yuan, C. A. van Blitterswijk, P. Habibovic, *Eur. Cells Mater.* **2011**, *21*, 407.

[4] a) Y. Zhang, J. Xu, Y. C. Ruan, M. K. Yu, M. O'Laughlin, H. Wise, D. Chen, L. Tian, D. Shi, J. Wang, S. Chen, J. Q. Feng, D. H. Chow, X. Xie, L. Zheng, L. Huang, S. Huang, K. Leung, N. Lu, L. Zhao, H. Li, D. Zhao, X. Guo, K. Chan, F. Witte, H. C. Chan, Y. Zheng, L. Qin, *Nat. Med.* **2016**, *22*, 1160; b) H. Qi, S. Heise, J. Zhou, K. Schuhladen, Y. Yang, N. Cui, R. Dong, S. Virtanen, Q. Chen, A. R. Boccaccini, T. Lu, *ACS Appl. Mater. Interfaces* **2019**, *11*, 8625; c) B. Li, P. Gao, H. Zhang, Z. Guo, Y. Zheng, Y. Han, *Biomater. Sci.* **2018**, *6*, 3202.

[5] a) C. Combes, C. Rey, *Acta Biomater.* **2010**, *6*, 3362; b) J. Tao, D. Zhou, Z. Zhang, X. Xu, R. Tang, *Proc. Natl. Acad. Sci. USA* **2009**, *106*, 22096; c) H. C. Ding, H. H. Pan, X. R. Xu, R. K. Tang, *Cryst. Growth Des.* **2014**, *14*, 763.

[6] J. H. de Baaij, J. G. Hoenderop, R. J. Bindels, *Physiol. Rev.* **2015**, *95*, 1.

[7] R. K. Rude, F. R. Singer, H. E. Gruber, *J. Am. Coll. Nutr.* **2009**, *28*, 131.

[8] S. Sprio, A. Ruffini, F. Valentini, T. D'Alessandro, M. Sandri, S. Panseri, A. Tampieri, *J. Biotechnol.* **2011**, *156*, 347.

[9] J. T. Richtsmeier, K. Flaherty, *Acta Neuropathol.* **2013**, *125*, 469.

[10] M. Ishii, A. E. Merrill, Y. S. Chan, I. Gitelman, D. P. Rice, H. M. Sucov, R. E. Maxson Jr., *Development* **2003**, *130*, 6131.

[11] L. A. Opperman, *Dev. Dyn.* **2000**, *219*, 472.

[12] a) F. Y. Li, B. Chaigne-Delalande, C. Kanellopoulou, J. C. Davis, H. F. Matthews, D. C. Douek, J. I. Cohen, G. Uzel, H. C. Su, M. J. Lenardo, *Nature* **2011**, *475*, 471; b) M. P. Staiger, A. M. Pietak, J. Huadmai, G. Dias, *Biomaterials* **2006**, *27*, 1728.

[13] A. Laskus, J. Kolmas, *Int. J. Mol. Sci.* **2017**, *18*, 2542.

[14] Y. Li, J. Wang, J. Yue, Y. Wang, C. Yang, Q. Cui, *Cell Biol. Int.* **2018**, *42*, 205.

[15] a) Z. Geng, Z. D. Cui, Z. Y. Li, S. L. Zhu, Y. Q. Liang, W. W. Lu, X. J. Yang, *J. Mater. Chem. B* **2015**, *3*, 3738; b) T. P. Feenstra, J. Hop, P. L. Debruyn, *J. Colloid Interface Sci.* **1981**, *83*, 583.

[16] a) X. Fu, Y. Li, T. Huang, Z. Yu, K. Ma, M. Yang, Q. Liu, H. Pan, H. Wang, J. Wang, M. Guan, *Adv. Sci.* **2018**, *5*, 1700755; b) J. L. Sun, K. Jiao, L. N. Niu, Y. Jiao, Q. Song, L. J. Shen, F. R. Tay, J. H. Chen, *Biomaterials* **2017**, *113*, 203.

[17] a) J. Mahamid, A. Sharir, D. Gur, E. Zelzer, L. Addadi, S. Weiner, *J. Struct. Biol.* **2011**, *174*, 527; b) L. Schmidt, A. Taiyab, V. S. Melvin, K. L. Jones, T. Williams, *Dis. Models Mech.* **2018**, *11*, dmm031526.

[18] a) I. Pilchova, K. Klacanova, Z. Tatarkova, P. Kaplan, P. Racay, *Oxid. Med. Cell. Longevity* **2017**, *2017*, 1; b) S. Boonrungsiman, E. Gentleman, R. Carzaniga, N. D. Evans, D. W. McComb, A. E. Porter, M. M. Stevens, *Proc. Natl. Acad. Sci. USA* **2012**, *109*, 14170.

[19] A. M. Romani, *Arch. Biochem. Biophys.* **2011**, *512*, 1.

[20] Y. Liu, Y. K. Kim, L. Dai, N. Li, S. O. Khan, D. H. Pashley, F. R. Tay, *Biomaterials* **2011**, *32*, 1291.

[21] R. H. G. Wright, F. Le Dily, M. Beato, *Trends Biochem. Sci.* **2019**, *44*, 565.

[22] M. C. Ting, N. L. Wu, P. G. Roybal, J. J. Sun, L. Q. Liu, Y. Z. Yen, R. E. Maxson, *Development* **2009**, *136*, 855.

[23] a) D. Lee, P. N. Kumta, *Mater. Sci. Eng., C* **2010**, *30*, 934; b) C. Shao, R. Zhao, S. Jiang, S. Yao, Z. Wu, B. Jin, Y. Yang, H. Pan, R. Tang, *Adv. Mater.* **2018**, *30*, 1704876; c) A. Romani, *Arch. Biochem. Biophys.* **2007**, *458*, 90.

[24] Y. Wang, T. Azais, M. Robin, A. Vallee, C. Catania, P. Legriel, G. Pehau-Arnaudet, F. Babonneau, M. M. Giraud-Guille, N. Nassif, *Nat. Mater.* **2012**, *11*, 724.

[25] Y. Liu, S. A. Liu, D. Luo, Z. J. Xue, X. A. Yang, L. Cu, Y. H. Zhou, T. Wang, *Adv. Mater.* **2016**, *28*, 8740.

[26] a) L. Louvet, L. Metzinger, J. Buchel, S. Steppan, Z. A. Massy, *Biomed. Res. Int.* **2016**, *2016*, 7419524; b) J. Kingman, J. Uitto, Q. Li, *Oncotarget* **2017**, *8*, 38152.

[27] I. Slutsky, N. Abumaria, L. J. Wu, C. Huang, L. Zhang, B. Li, X. Zhao, A. Govindarajan, M. G. Zhao, M. Zhuo, S. Tonegawa, G. Liu, *Neuron* **2010**, *65*, 165.

[28] J. M. Diaz-Tocados, C. Herencia, J. M. Martinez-Moreno, A. M. de Oca, M. E. Rodriguez-Ortiz, N. Vergara, A. Blanco, S. Steppan, Y. Almaden, M. Rodriguez, J. R. Munoz-Castaneda, *Sci. Rep.* **2017**, *7*, 7839.

[29] N. S. Dole, C. M. Mazur, C. Acevedo, J. P. Lopez, D. A. Monteiro, T. W. Fowler, B. Gludovatz, F. Walsh, J. N. Regan, S. Messina, D. S. Evans, T. F. Lang, B. Zhang, R. O. Ritchie, K. S. Mohammad, T. Alliston, *Cell Rep.* **2017**, *21*, 2585.

[30] S. E. Turecamo, T. A. Walji, T. J. Broekelmann, J. W. Williams, S. Ivanov, N. K. Wee, J. D. Procknow, M. R. McManus, G. J. Randolph, E. L. Scheller, R. P. Mecham, C. S. Craft, *Matrix Biol.* **2018**, *67*, 1.